Human-Graded Rocket Stage Landing via Robotic Capture, Active Landing Legs, and Translating Hydraulic Platform

Dinesh Appavoo, B.Tech, MS, MS
Hypersona Inc.
hello@dineshappavoo.com

Abstract: This paper presents a multi-layered hydraulic attenuation system designed for the controlled vertical landing of a crewed rocket second stage (Stage 2). The proposed architecture integrates three independently controlled, actively damped subsystems—a robotic catching arm assembly mounted on a vertical tower, hydraulic landing legs affixed to the rocket structure, and a translating hydraulic landing platform—to distribute the deceleration impulse over an extended distance and time interval. By coupling three active hydraulic stroke elements with a cumulative deceleration distance of $d_{\text{arm}} + d_{\text{leg}} + d_{\text{pad}}$, peak acceleration experienced by the crew is maintained within proposed human-graded limits, referenced against NASA's established crew tolerance criteria of $3\,g$ sustained and $6\,g$ transient loading [1]. A physics-based analysis grounded in the impulse-momentum theorem demonstrates that translating the landing surface concurrently with the descending vehicle substantially reduces the net impulsive force compared to a static landing surface. A feedback control architecture employing hydraulic utilization monitoring governs the coordinated response of all three subsystems through three distinct operational phases: powered descent to arm capture, arm-guided descent to platform contact, and fully hydraulic deceleration to rest. The three-layer redundancy provides progressive safety margins and contingency capacity for off-nominal arrival conditions. System-level force balance equations, energy dissipation models, and control laws are derived using symbolic parameters and validated against human tolerance boundaries.

I. System Overview and Objectives

The recovery and reuse of rocket stages represents a transformative capability in space transportation. While first-stage booster recovery has been demonstrated through propulsive vertical landing [7], the recovery of a crewed second stage—henceforth referred to as Stage 2—introduces stringent constraints on the deceleration environment experienced during touchdown. For a human-rated landing system, the peak acceleration must remain within physiological tolerance limits throughout the entirety of the landing event [1, 9].

This paper proposes a landing architecture that employs three coordinated, actively controlled hydraulic subsystems to distribute the landing impulse over a substantially greater distance and time interval than any single mechanism could achieve independently. The fundamental physics principle underlying this approach is rooted in the impulse-momentum theorem [2]: when a landing surface translates in the direction of the descending vehicle's motion during the moment of contact, the relative velocity between the vehicle and the surface is reduced, thereby diminishing the impulsive force transmitted to the structure and its occupants.

The proposed system comprises three principal elements, illustrated schematically in Fig. 1:

1. **Robotic Catching Tower with Hydraulic Arms:** A tower structure positioned adjacent to the landing site, taller than the Stage 2 vehicle, equipped with two robotic arms that capture the vehicle at structural hard points located near the top of the stage. The arms translate vertically on hydraulically damped carriages with a maximum stroke distance d_{arm}.
2. **Active Hydraulic Landing Legs:** Landing legs mounted to the base of Stage 2, each incorporating a controlled (variable-orifice) hydraulic shock absorber with a maximum stroke distance d_{leg}. These legs serve as the primary energy absorption interface upon contact with the landing platform.
3. **Translating Hydraulic Landing Platform:** A ground-based platform that translates vertically downward upon contact with the rocket's landing legs, driven by a controlled hydraulic actuation system with a maximum stroke distance d_{pad}.

The total available deceleration distance is therefore:

$$d_{\text{total}} = d_{\text{arm}} + d_{\text{leg}} + d_{\text{pad}} \tag{1}$$

The operational concept proceeds through three phases. In Phase 1, the rocket descends under engine thrust and gimbal control toward the catching tower. In Phase 2, the robotic arms capture the vehicle, and the combined system of arm damping and engine thrust guide the rocket downward toward the landing platform. In Phase 3, the landing legs contact the platform, the engine transitions to idle, and the three hydraulic subsystems absorb the remaining kinetic energy to bring the vehicle to rest. This phased approach ensures that at no point during the landing sequence does the crew experience accelerations exceeding the proposed human-graded limits.

Nomenclature

a	Acceleration ($\mathrm{m/s^2}$)
$a_{\max}$	Maximum allowable acceleration ($\mathrm{m/s^2}$)
A_{v}	Variable orifice area ($\mathrm{m^2}$)
A_p	Piston area ($\mathrm{m^2}$)
c	Damping coefficient
C_{d}	Discharge coefficient
d_{arm}	Arm carriage stroke distance (m)
d_{leg}	Landing leg stroke distance (m)
d_{pad}	Platform stroke distance (m)
$e(t)$	Control error signal
F	Force (N)
g	Gravitational acceleration ($9.81\,\mathrm{m/s^2}$)
$j_{\max}$	Maximum jerk ($\mathrm{m/s^3}$)
K_p, K_i, K_d	PID controller gains
m_{r}	Rocket mass (kg)
n	Velocity exponent
N_{legs}	Number of landing legs
v_{r}	Rocket descent velocity (m/s)
η	Hydraulic utilization ratio
ρ	Hydraulic fluid density ($\mathrm{kg/m^3}$)
θ_{leg}	Landing leg inclination angle (rad)

II. Component Analysis and Governing Equations

This section presents the physics and governing equations for each subsystem. All three subsystems employ controlled hydraulic damping as the primary energy dissipation mechanism. We first develop the unified hydraulic damper model, then specialize it for each component.

A. Controlled Hydraulic Damper: Unified Model

A hydraulic damper dissipates kinetic energy by forcing fluid through an orifice, converting mechanical energy to thermal energy via viscous losses. For a controlled (variable-orifice) damper, the orifice area A_{v} can be modulated in real time to vary the damping force [3, 4].

The instantaneous damping force produced by a hydraulic damper is given by the orifice flow equation derived from Bernoulli's principle [4]:

$$F_{\mathrm{d}} = \frac{\rho\, A_p^2}{2\, C_{\mathrm{d}}^2\, A_{\mathrm{v}}^2}\, \dot{x}^2 \tag{2}$$

where ρ is the hydraulic fluid density, A_p is the piston area, C_{d} is the discharge coefficient (typically 0.6–0.7) [4], A_{v} is the variable orifice area, and $\dot{x}$ is the piston velocity. The quadratic velocity dependence arises from the turbulent flow regime characteristic of high-velocity impact events.

For control purposes, it is convenient to express the damping force in the generalized form:

$$F_{\mathrm{d}} = c(A_{\mathrm{v}})\, \dot{x}^{\,n} \tag{3}$$

where $c(A_{\mathrm{v}})$ is the controllable damping coefficient that depends on the orifice area, and n is the velocity exponent ($n = 2$ for fully turbulent flow, $n = 1$ for laminar flow) [3]. In practice, $1 \le n \le 2$ depending on the Reynolds number of the flow.

The energy dissipated by the hydraulic damper over a stroke d is:

$$E_{\mathrm{diss}} = \int_0^d F_{\mathrm{d}}\, dx = \int_0^d c(A_{\mathrm{v}})\, \dot{x}^{\,n}\, dx \tag{4}$$

The damping coefficient may be actively modulated by varying the orifice area according to a control law. For a proportional control scheme [5]:

$$A_{\mathrm{v}}(t) = A_{\mathrm{v}}^{*} + K_p\, e(t) + K_i \int_0^t e(\tau)\, d\tau + K_d\, \dot{e}(t) \tag{5}$$

where A_{v}^{*} is the nominal orifice area, $e(t)$ is the error signal (deviation from a desired state), and K_p, K_i, K_d are the proportional, integral, and derivative gains, respectively. The selection of these gains determines the transient response and stability of the damping system [5].

B. Impulse-Momentum Framework

The impulse-momentum theorem provides the fundamental relationship governing the landing event [2]. For a rocket of mass m_{r} decelerating from velocity v_1 to velocity v_2:

$$\int_{t_1}^{t_2} F(t)\, dt = m_{\mathrm{r}}\, (v_2 - v_1) \tag{6}$$

The average force experienced during the landing is:

$$\bar{F} = \frac{m_{\mathrm{r}}\, \Delta v}{\Delta t} \tag{7}$$

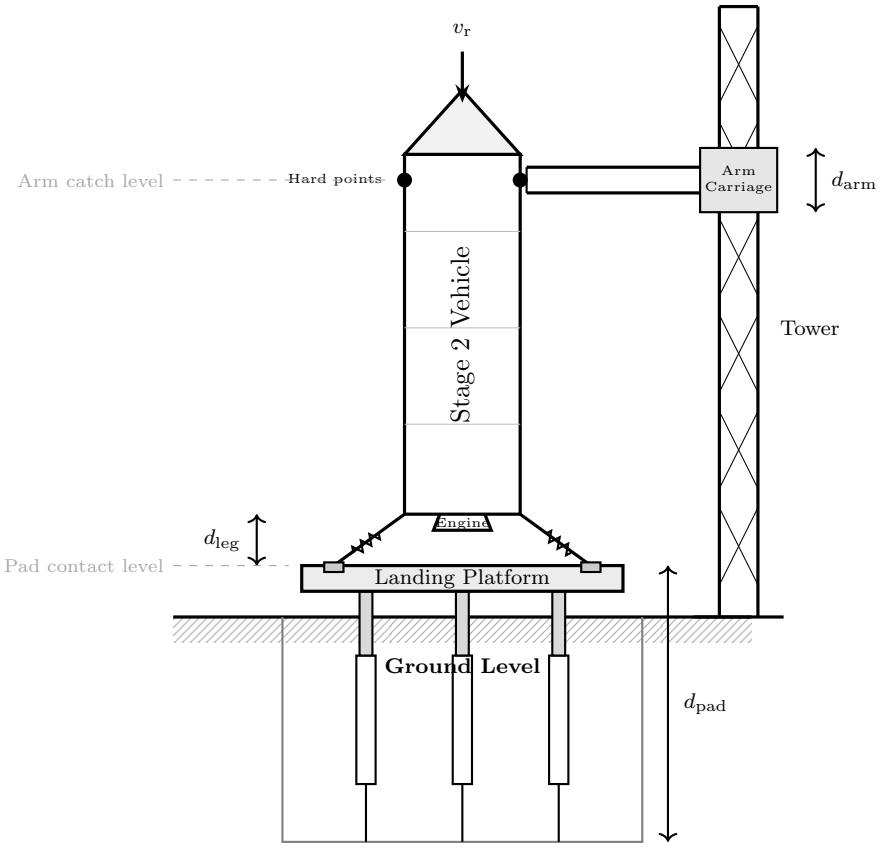

Figure 1: Schematic of the multi-layered landing system showing the three hydraulic subsystems: robotic catching arms (stroke d_{arm}), active landing legs (stroke d_{leg}), and translating hydraulic platform (stroke d_{pad}). The Stage 2 vehicle descends with velocity v_{r} toward the catching tower.

When the landing surface translates with velocity v_{pad} in the same direction as the rocket's descent velocity v_{r}, the relative velocity at contact is:

$$v_{\text{rel}} = v_{\text{r}} - v_{\text{pad}} \tag{8}$$

The momentum change experienced by the rocket upon engaging with a moving surface is proportional to this relative velocity rather than the absolute velocity. The impulsive force is therefore [2]:

$$F_{\text{impulse}} = \frac{m_{\text{r}}\, v_{\text{rel}}}{\Delta t} = \frac{m_{\text{r}}\,(v_{\text{r}} - v_{\text{pad}})}{\Delta t} \tag{9}$$

This is the central physical insight: by designing a landing surface that moves with the descending rocket at the moment of contact, the effective impulsive force is reduced by a factor of $(v_{\text{r}} - v_{\text{pad}})/v_{\text{r}}$ compared to a static surface. This principle extends to all three subsystems—each one contributes to reducing the relative velocity at its respective interface.

C. Work-Energy Dissipation Across Three Subsystems

By the work-energy theorem [2], the total kinetic energy of the descending rocket must be dissipated by the combined action of all active subsystems plus any residual engine thrust:

$$\frac{1}{2} m_{\text{r}}\, v_0^2 = E_{\text{arm}} + E_{\text{leg}} + E_{\text{pad}} + W_{\text{thrust}} + W_{\text{gravity}} \tag{10}$$

where v_0 is the rocket velocity at the moment of arm capture, E_{arm}, E_{leg}, and E_{pad} are the energies dissipated by the respective hydraulic subsystems (each computed via Eq. (4)), W_{thrust} is the work performed by engine thrust during the descent (prior to idle transition at pad contact), and W_{gravity} is the work done by gravity over the total descent distance.

The gravitational work term is:

$$W_{\text{gravity}} = m_{\text{r}}\, g\, d_{\text{total}} \tag{11}$$

where g is gravitational acceleration. Note that gravity acts in the direction of motion (downward), adding energy to the system that must be absorbed.

Including gravity, the full energy balance becomes:

$$\frac{1}{2}m_{\mathrm{r}}\,v_0^2+m_{\mathrm{r}}\,g\,d_{\mathrm{total}}=E_{\mathrm{arm}}+E_{\mathrm{leg}}+E_{\mathrm{pad}}+W_{\mathrm{thrust}} \quad (12)$$

D. Robotic Catching Arms

The catching tower is a vertical structure of height H_{tower}, satisfying $H_{\mathrm{tower}} > H_{\mathrm{rocket}} + d_{\mathrm{arm}} + \delta_{\mathrm{margin}}$, where H_{rocket} is the height of the Stage 2 vehicle and δ_{margin} is a safety margin. Two robotic arms extend horizontally from a carriage that rides on vertical hydraulic rails.

The arm carriage is actuated by a controlled hydraulic system. Upon capturing the rocket at the structural hard points, the carriage begins its downward stroke. The equation of motion for the arm carriage during Phase 2 is obtained from Newton's second law [2]:

$$(m_{\mathrm{r}}+m_{\mathrm{arm}})\,\ddot{x}_{\mathrm{arm}}=(m_{\mathrm{r}}+m_{\mathrm{arm}})\,g+F_{\mathrm{thrust}}-F_{\mathrm{d,arm}} \quad (13)$$

where m_{arm} is the mass of the arm carriage assembly, $\ddot{x}_{\mathrm{arm}}$ is the downward acceleration, F_{thrust} is the upward engine thrust (with the sign convention that positive is downward), and $F_{\mathrm{d,arm}}$ is the hydraulic damping force from the arm's controlled damper (Eq. (2)).

The damping force for the arm hydraulic system is:

$$F_{\mathrm{d,arm}}=c_{\mathrm{arm}}(A_{\mathrm{v}}^{\mathrm{arm}})\,\dot{x}_{\mathrm{arm}}^{\,n} \quad (14)$$

The maximum deceleration experienced during the arm-guided phase must satisfy:

$$|\ddot{x}_{\mathrm{arm}}|\le a_{\max} \quad (15)$$

where $a_{\max}$ is the human tolerance acceleration limit (proposed at $3g$ for sustained loading) [1].

E. Active Hydraulic Landing Legs

Each landing leg incorporates a controlled hydraulic shock absorber that compresses upon contact with the landing platform. For N_{legs} landing legs, each inclined at angle θ_{leg} from the vertical, the vertical component of the total damping force is [10]:

$$F_{\mathrm{d,leg}}=N_{\mathrm{legs}}\,c_{\mathrm{leg}}(A_{\mathrm{v}}^{\mathrm{leg}})\,(\dot{x}_{\mathrm{leg}}\cos\theta_{\mathrm{leg}})^n\,\cos\theta_{\mathrm{leg}} \quad (16)$$

The *hydraulic utilization ratio* for the landing legs is defined as:

$$\eta_{\mathrm{leg}}(t)=\frac{x_{\mathrm{leg}}(t)}{d_{\mathrm{leg}}} \quad (17)$$

where $x_{\mathrm{leg}}(t)$ is the current stroke displacement and d_{leg} is the maximum allowable stroke. This ratio serves as the primary feedback signal for the coordinated control system (see Section 2.7).

The energy absorbed by the landing legs is:

$$E_{\mathrm{leg}}=N_{\mathrm{legs}}\int_0^{d_{\mathrm{leg}}}c_{\mathrm{leg}}(A_{\mathrm{v}}^{\mathrm{leg}})\,(\dot{x}_{\mathrm{leg}}\cos\theta_{\mathrm{leg}})^n\,\cos\theta_{\mathrm{leg}}\,dx_{\mathrm{leg}} \quad (18)$$

F. Translating Hydraulic Landing Platform

The landing platform is a rigid surface mounted on a hydraulic actuation system that permits controlled vertical translation over a stroke distance d_{pad}. Upon receiving the signal that the landing legs have made contact (via force/pressure sensors in the legs), the platform controller engages.

The equation of motion for the platform is:

$$(m_{\mathrm{pad}}+m_{\mathrm{r}})\,\ddot{x}_{\mathrm{pad}}=(m_{\mathrm{r}}+m_{\mathrm{pad}})\,g-F_{\mathrm{d,pad}}-F_{\mathrm{d,leg}} \quad (19)$$

where m_{pad} is the platform mass and $F_{\mathrm{d,pad}}$ is the platform's hydraulic damping force:

$$F_{\mathrm{d,pad}}=c_{\mathrm{pad}}(A_{\mathrm{v}}^{\mathrm{pad}})\,\dot{x}_{\mathrm{pad}}^{\,n} \quad (20)$$

The platform utilization ratio is:

$$\eta_{\mathrm{pad}}(t)=\frac{x_{\mathrm{pad}}(t)}{d_{\mathrm{pad}}} \quad (21)$$

G. Coordinated Feedback Control System

The three subsystems are coordinated through a hierarchical control architecture [5, 6]. The control law governing the platform velocity response is linked to the leg utilization ratio:

$$v_{\mathrm{pad}}(t)=\begin{cases}v_{\mathrm{pad,nom}} & \text{if } \eta_{\mathrm{leg}}\le\eta_{\mathrm{thresh}}\\ v_{\mathrm{pad,nom}}+K_{\mathrm{pad}}\,(\eta_{\mathrm{leg}}-\eta_{\mathrm{thresh}}) & \text{if } \eta_{\mathrm{leg}}>\eta_{\mathrm{thresh}}\end{cases} \quad (22)$$

where η_{thresh} is the utilization threshold (proposed at 0.75), $v_{\mathrm{pad,nom}}$ is the nominal platform descent velocity, and K_{pad} is the proportional gain. The platform velocity is bounded:

$$0\le v_{\mathrm{pad}}(t)\le v_{\mathrm{pad,max}} \quad (23)$$

Similarly, the arm subsystem provides an intervention response during Phase 3 if the rocket velocity remains excessive as the platform approaches its stroke limit:

$$F_{\mathrm{arm,intervene}}=K_{\mathrm{arm}}\,(\eta_{\mathrm{pad}}-\eta_{\mathrm{pad,crit}})\,v_{\mathrm{r}}(t) \quad (24)$$

where $\eta_{\mathrm{pad,crit}}$ is a critical platform utilization threshold (e.g., 0.85) beyond which the arms re-engage to provide supplementary deceleration force.

The deceleration profile for the final approach to rest must satisfy the jerk constraint [12]:

$$\left|\frac{da}{dt}\right|\le j_{\max} \quad (25)$$

where a is the acceleration and $j_{\max}$ is the maximum allowable jerk. Minimizing jerk produces a smooth deceleration profile and is essential for crew comfort and structural integrity [12].

The optimal deceleration profile to bring the rocket from velocity v to rest over a remaining distance d_{rem} with bounded acceleration and jerk is described by a trapezoidal acceleration profile [13]:

$$a(t) = \begin{cases} j_{\max}\, t & 0 \le t \le t_1 \\ a_{\max} & t_1 < t \le t_2 \\ a_{\max} - j_{\max}(t - t_2) & t_2 < t \le t_3 \end{cases} \tag{26}$$

where t_1, t_2, and t_3 are determined by the boundary conditions $v(t_3) = 0$ and $\int_0^{t_3} v(t)\, dt = d_{\text{rem}}$ [13].

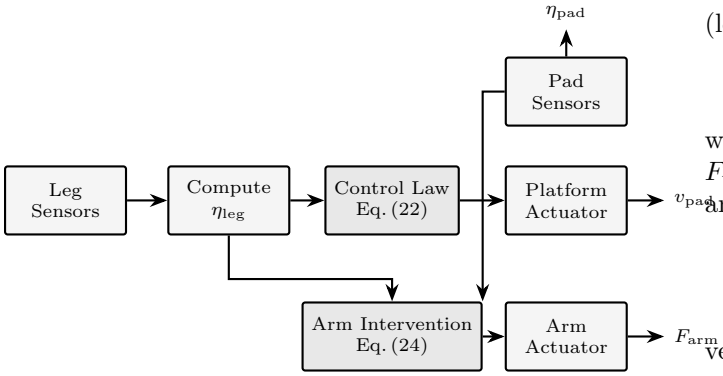

Figure 2: Feedback control architecture. Landing leg sensor data drives both the platform velocity control and the arm intervention logic. Pad utilization feeds back to the arm controller.

H. Human Tolerance Criteria

NASA-STD-3001, Volume 2 [1] and associated research by Eiband [11] establish the following crew tolerance limits for seated, restrained occupants with vertical ($+G_z$) loading:

$$a_{\text{sustained}} \le 3g, \quad a_{\text{transient}} \le 6g \tag{27}$$

The duration of transient loading must satisfy the Eiband curve criteria, which relates peak acceleration magnitude to pulse duration [11]. For the proposed system, the design requirement is:

$$\max_t |a(t)| \le 3g \quad \forall\, t \in [t_{\text{catch}},\, t_{\text{stop}}] \tag{28}$$

under nominal conditions, with the $6g$ transient limit serving as the off-nominal boundary.

III. Operational Landing Sequence

This section describes the complete landing sequence from atmospheric entry to full stop. The operational timeline is divided into three distinct phases, each governed by different combinations of the active subsystems.

A. Phase 1: Powered Descent to Arm Capture

Stage 2 executes a deorbit burn and enters the atmosphere on a trajectory toward the landing site. During the terminal descent phase, the vehicle performs a *landing burn* using its main engine(s) and gimbal control to decelerate and guide itself toward the catching tower's capture envelope [7, 8].

The equations of motion during powered descent, neglecting aerodynamic forces near the terminal phase (low velocity, near sea level), are [2]:

$$m_{\text{r}}\, \ddot{z} = F_{\text{thrust}} - m_{\text{r}}\, g \tag{29}$$

where z is the vertical coordinate (positive upward), and F_{thrust} is the thrust force directed upward. The gimbal angle δ_g provides lateral control:

$$m_{\text{r}}\, \ddot{y} = F_{\text{thrust}} \sin \delta_g \tag{30}$$

The vehicle must arrive at the capture point with velocity v_{r} within the admissible capture envelope:

$$v_{\min} \le |v_{\text{r}}(t_{\text{catch}})| \le v_{\max} \tag{31}$$

and lateral position error within the arm reach:

$$|\Delta y(t_{\text{catch}})| \le L_{\text{arm}} - r_{\text{rocket}} - \delta_{\text{clearance}} \tag{32}$$

where L_{arm} is the arm length, r_{rocket} is the rocket radius, and $\delta_{\text{clearance}}$ is a safety clearance.

B. Phase 2: Arm-Guided Descent to Platform Contact

At time t_{catch}, the robotic arms engage the structural hard points at the top of Stage 2. The arms clamp onto the vehicle, and the arm carriage begins its controlled descent along the tower rails.

During this phase, both the arm hydraulic damping and the engine thrust (still active) contribute to decelerating the vehicle. The governing equation is Eq. (13). The engine thrust is modulated to maintain the descent velocity within the desired profile:

$$F_{\text{thrust}}(t) = (m_{\text{r}} + m_{\text{arm}})(g - a_{\text{des}}) + F_{\text{d,arm}} \tag{33}$$

where a_{des} is the desired deceleration (positive upward), constrained by Eq. (15).

The velocity at the end of Phase 2 (platform contact) is:

$$v_{\text{contact}} = \sqrt{v_0^2 - 2\,\bar{a}_{\text{P2}}\,d_{\text{arm}}} \tag{34}$$

where $\bar{a}_{\text{P2}}$ is the average net deceleration during Phase 2, assuming approximately constant deceleration (a simplification for design purposes).

C. Phase 3: Hydraulic Deceleration to Rest

At pad contact ($t = t_{\text{contact}}$), the following sequence occurs:

Step 1: Force/pressure sensors in the landing legs detect contact and transmit a signal to the platform controller.

Step 2: The engine transitions to idle. Thrust force drops to a minimal idle value $F_{\text{thrust}} \approx 0$ (engine remains in ready state for contingency use).

Step 3: The landing leg hydraulic absorbers begin compressing, absorbing energy per Eq. (16).

Step 4: Simultaneously, the platform controller activates the platform descent per the control law in Eq. (22).

The combined equation of motion during Phase 3 is:

$$m_{\text{r}}\,\ddot{x} = m_{\text{r}}\,g - F_{\text{d,leg}} - F_{\text{d,pad}} - F_{\text{arm,intervene}} \tag{35}$$

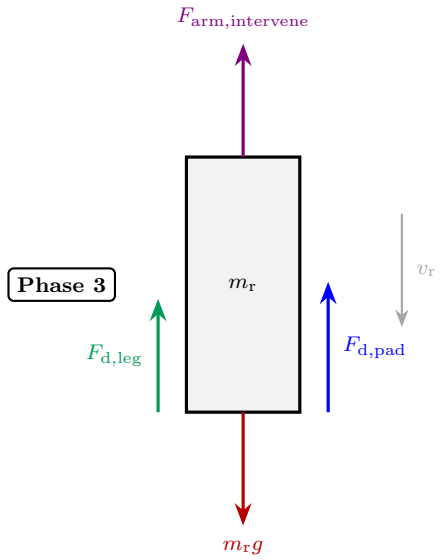

Figure 3: Free body diagram during Phase 3. Gravity ($m_{\text{r}}g$, downward) acts against the three hydraulic subsystem forces: landing leg damping $F_{\text{d,leg}}$, platform damping $F_{\text{d,pad}}$, and arm intervention $F_{\text{arm,intervene}}$ (all upward). The rocket descends with velocity v_{r}.

The deceleration at any instant during Phase 3 is:

$$a(t) = g - \frac{F_{\text{d,leg}} + F_{\text{d,pad}} + F_{\text{arm,intervene}}}{m_{\text{r}}} \tag{36}$$

The condition for a safe landing is:

$$|a(t)| \le 3g \quad \Rightarrow \quad F_{\text{d,leg}} + F_{\text{d,pad}} + F_{\text{arm,intervene}} \le 4\,m_{\text{r}}\,g \tag{37}$$

(The factor $4g$ arises because gravity contributes $1g$ downward, so a $3g$ upward net deceleration requires total upward force equal to $4\,m_{\text{r}}\,g$.)

IV. Analytical Description of the Landing Sequence

We now trace through the entire landing sequence, linking each physical event to the governing equations derived in Section 2.

A. Entry Conditions and Capture

The rocket approaches the landing site with the main engine(s) firing. The thrust-to-weight ratio during the landing burn is selected to produce the desired deceleration profile per Eq. (29). The vehicle's guidance system steers toward the capture envelope defined by Eqs. (31)–(32).

Let the velocity at arm capture be v_0. The kinetic energy at this instant is:

$$K_0 = \frac{1}{2} m_{\text{r}}\,v_0^2 \tag{38}$$

This energy, plus the gravitational potential energy gained during the subsequent descent ($m_{\text{r}}\,g\,d_{\text{total}}$), must be fully dissipated by the three hydraulic subsystems per the energy balance in Eq. (12).

B. Arm-Guided Descent (Phase 2 Analysis)

Upon capture, the arm carriage and rocket descend together. The equation of motion is Eq. (13), with the arm damping force controlled via Eq. (14). The engine thrust is simultaneously adjusted per Eq. (33) to maintain the desired deceleration profile.

The energy dissipated by the arms during Phase 2 is:

$$E_{\text{arm}} = \int_0^{d_{\text{arm}}} F_{\text{d,arm}}\,dx = \int_0^{d_{\text{arm}}} c_{\text{arm}}\,\dot{x}_{\text{arm}}^{\,n}\,dx \tag{39}$$

The work done by engine thrust during Phase 2 is:

$$W_{\text{thrust}} = \int_0^{d_{\text{arm}}} F_{\text{thrust}}(x)\,dx \tag{40}$$

Note that the engine thrust acts *upward* (opposing motion), so W_{thrust} contributes positively to energy removal. The velocity at pad contact is given by Eq. (34).

C. Pad Contact and Hydraulic Deceleration (Phase 3 Analysis)

At pad contact, the engine transitions to idle. The rocket now has velocity v_{contact} and must be brought to rest over the combined remaining stroke of $d_{\text{leg}} + d_{\text{pad}}$.

The landing leg sensors detect contact and transmit the signal to the platform controller. The leg hydraulic absorbers engage immediately, producing the force given by Eq. (16). The platform hydraulic system activates per the control law in Eq. (22).

Utilization-Based Feedback Loop: As the legs compress, the utilization ratio η_{leg} (Eq. (17)) is monitored continuously. If η_{leg} exceeds the threshold $\eta_{\text{thresh}} = 0.75$, the platform velocity increases proportionally (Eq. (22)), effectively increasing the rate at which the landing surface retreats from the descending vehicle. This reduces the compression rate of the landing legs, preventing premature stroke exhaustion.

Arm Intervention: If the platform utilization η_{pad} (Eq. (21)) approaches its critical value $\eta_{\text{pad,crit}}$, the arm intervention force (Eq. (24)) activates, providing supplementary deceleration from the top of the vehicle. This constitutes the third layer of protection.

D. Final Deceleration to Rest

The final phase of the landing requires careful coordination to bring the vehicle to rest ($v = 0$) at precisely the moment when the stroke limits are reached. This requires the deceleration profile to follow the trapezoidal trajectory defined by Eq. (26), satisfying both the jerk limit (Eq. (25)) and the acceleration limit (Eq. (28)).

The terminal condition for a successful landing is:

$$v_{\text{r}}(t_{\text{stop}}) = 0, \quad \eta_{\text{leg}}(t_{\text{stop}}) \leq 1.0, \quad \eta_{\text{pad}}(t_{\text{stop}}) \leq 1.0 \tag{41}$$

At the point of full stop, it is acceptable (and by design, expected) that both the leg and pad hydraulic systems approach full utilization ($\eta \approx 1.0$), provided the velocity reaches zero simultaneously. The safest deceleration profile to achieve this is determined by solving the optimal control problem:

Minimize: $\max_t |a(t)|$

Subject to:

$$\int_0^{t_{\text{stop}}} v(t)\, dt = d_{\text{leg}} + d_{\text{pad}} \tag{42}$$

$$v(t_{\text{stop}}) = 0 \tag{43}$$

$$|a(t)| \leq 3g \tag{44}$$

$$\left|\frac{da}{dt}\right| \leq j_{\max} \tag{45}$$

This optimal control formulation produces the trapezoidal acceleration profile of Eq. (26) [13].

V. Three Levels of Protection

A distinguishing feature of the proposed landing architecture is the inherent three-layer redundancy. Each hydraulic subsystem constitutes an independent level of protection, and the system is designed such that any single subsystem can partially compensate for degraded performance in another. This section highlights the protective hierarchy and its implications for safety margins.

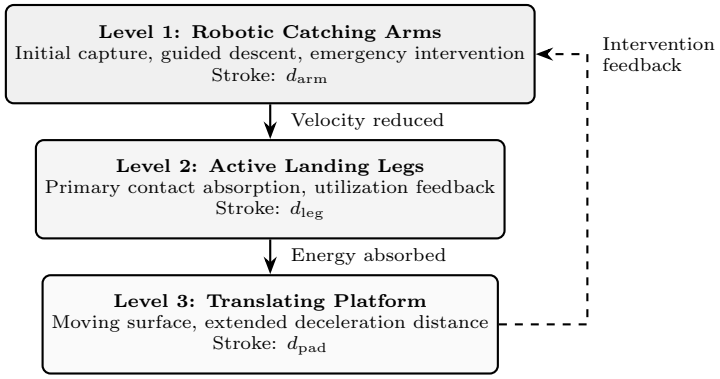

Figure 4: Three levels of protection. Each layer reduces the velocity and energy burden on subsequent layers. The dashed feedback loop enables arm intervention when platform utilization approaches critical limits.

A. Level 1: Robotic Catching Arms

The catching arms serve as the first point of contact and provide three distinct protective functions: (a) lateral stabilization and alignment correction, (b) initial deceleration during the arm-guided descent in Phase 2, and (c) emergency intervention during Phase 3 if the lower subsystems approach their limits. The arms represent the highest-authority safety mechanism because they engage earliest and can re-engage during the final phase.

B. Level 2: Active Landing Legs

The variable-orifice hydraulic landing legs provide the primary energy absorption at pad contact. Their controlled damping coefficient allows real-time adaptation to the actual contact velocity, which may deviate from the nominal design point. The utilization feedback signal (η_{leg}, Eq. (17)) serves as the master control signal for the entire Phase 3 coordination.

C. Level 3: Translating Hydraulic Platform

The translating platform embodies the core physics innovation of this system. By moving the landing surface downward at the moment of contact, the effective relative velocity is reduced per Eq. (8), and the deceleration

distance is extended by d_{pad}. Even if the landing legs were to reach full utilization, the platform can continue absorbing energy independently.

D. Redundancy and Off-Nominal Performance

The total available deceleration distance (Eq. (1)) provides a safety margin that accommodates off-nominal arrival conditions. Consider the case where the velocity at arm capture exceeds the nominal value by a fraction α:

$$v_0' = (1+\alpha)\, v_0 \tag{46}$$

The kinetic energy increases by a factor of $(1+\alpha)^2$:

$$K_0' = (1+\alpha)^2\, K_0 \tag{47}$$

For $\alpha = 0.10$ (10% velocity exceedance), the energy increase is 21%. The three-layer system can accommodate this through a combination of: (a) increased arm damping force (by reducing $A_{\text{v}}^{\text{arm}}$), (b) increased leg damping coefficient, and (c) increased platform travel velocity up to $v_{\text{pad,max}}$. The system's capacity to absorb off-nominal energy without exceeding the $3g$ sustained limit is determined by the combined stroke budget:

$$E_{\max} = \int_0^{d_{\text{arm}}} F_{\text{d,arm}}^{\max}\, dx + \int_0^{d_{\text{leg}}} F_{\text{d,leg}}^{\max}\, dx + \int_0^{d_{\text{pad}}} F_{\text{d,pad}}^{\max}\, dx \tag{48}$$

where $F^{\max}$ denotes the maximum damping force each subsystem can produce while keeping instantaneous acceleration below $3g$.

The landing system is considered to have adequate margin when:

$$E_{\max} \geq (1+\alpha_{\text{margin}})^2\, K_0 + m_{\text{r}}\, g\, d_{\text{total}} \tag{49}$$

where α_{margin} is the design velocity margin factor.

If the arrival velocity exceeds all safety margins and the system cannot maintain the $3g$ limit, the engine (held at idle during Phase 3) can be re-ignited as a final contingency. While this introduces additional forces and complexity, the availability of engine restart provides an ultimate safety backstop that further strengthens the human-graded designation.

VI. Conclusion

This paper has presented a multi-layered hydraulic attenuation system for human-graded rocket second-stage landing. The architecture integrates three actively controlled hydraulic subsystems—robotic catching arms, active landing legs, and a translating hydraulic landing platform—to distribute the landing impulse over a cumulative stroke distance of $d_{\text{arm}}+d_{\text{leg}}+d_{\text{pad}}$. The central physical principle, grounded in the impulse-momentum theorem, is that a landing surface translating in the direction of the descending vehicle reduces the relative velocity at contact and consequently the impulsive force experienced by the crew.

The coordinated feedback control system, driven by hydraulic utilization monitoring, provides real-time adaptation to the actual landing conditions. The three-phase operational sequence—powered descent to arm capture, arm-guided descent to platform contact, and fully hydraulic deceleration to rest—ensures that crew acceleration remains within proposed human-graded limits ($3g$ sustained, $6g$ transient) referenced against NASA-STD-3001 tolerance criteria.

The three-level protection hierarchy offers progressive redundancy: each layer independently contributes to energy absorption, and the feedback architecture enables cross-layer intervention when any subsystem approaches its operational limits. The system accommodates off-nominal arrival velocities through the combined stroke budget and variable damping coefficients, providing a quantifiable safety margin.

Future work should address detailed structural design of the catching tower and arm mechanism, high-fidelity dynamic simulation incorporating structural flexibility and hydraulic fluid compressibility, sensor fusion algorithms for real-time utilization estimation, and experimental validation through scaled prototype testing. Electromagnetic actuation for the precision control aspect of the catching arms merits investigation as an alternative or complement to the hydraulic approach.

References

[1] National Aeronautics and Space Administration, "NASA-STD-3001: NASA Space Flight Human-System Standard, Volume 2: Human Factors, Habitability, and Environmental Health," NASA Technical Standard, Rev. B, 2019.

[2] Meriam, J. L., Kraige, L. G., and Bolton, J. N., *Engineering Mechanics: Dynamics*, 9th ed., Wiley, Hoboken, NJ, 2020.

[3] Dixon, J. C., *The Shock Absorber Handbook*, 2nd ed., Wiley, Chichester, UK, 2007.

[4] Merritt, H. E., *Hydraulic Control Systems*, Wiley, New York, 1967.

[5] Ogata, K., *Modern Control Engineering*, 5th ed., Prentice Hall, Upper Saddle River, NJ, 2010.

[6] Franklin, G. F., Powell, J. D., and Emami-Naeini, A., *Feedback Control of Dynamic Systems*, 7th ed., Pearson, Upper Saddle River, NJ, 2015.

[7] Blackmore, L., "Autonomous Precision Landing of Space Rockets," *Annual Review of Control, Robotics, and Autonomous Systems*, Vol. 4, 2016, pp. 113–141.

[8] Açıkmeşe, B., and Ploen, S. R., "Convex Programming Approach to Powered Descent Guidance for Mars Landing," *Journal of Guidance, Control, and Dynamics*, Vol. 30, No. 5, 2007, pp. 1353–1366.

[9] Seedhouse, E., *SpaceX: Making Commercial Spaceflight a Reality*, Springer-Praxis, Chichester, UK, 2015.

[10] Currey, N. S., *Aircraft Landing Gear Design: Principles and Practices*, AIAA Education Series, Washington, DC, 1988.

[11] Eiband, A. M., "Human Tolerance to Rapidly Applied Accelerations: A Summary of the Literature," NASA Memorandum 5-19-59E, 1959.

[12] Flash, T., and Hogan, N., "The Coordination of Arm Movements: An Experimentally Confirmed Mathematical Model," *Journal of Neuroscience*, Vol. 5, No. 7, 1985, pp. 1688–1703.

[13] Biagiotti, L., and Melchiorri, C., *Trajectory Planning for Automatic Machines and Robots*, Springer, Berlin, 2008.